Structural stability of short-period Si/Ge superlattices studied with Raman spectroscopy

R. Schorer, E. Friess, K. Eberl, and G. Abstreiter
Walter Schottky Institut, Technische Universität München, D-8046 Garching, Federal Republic of Germany
(Received 17 December 1990; revised manuscript received 1 February 1991)

Annealing effects on strain-symmetrized Si/Ge superlattices with period lengths of 6 to 24 monolayers are studied by Raman spectroscopy in the temperature range of 430 °C to 780 °C. Using a simple microscopic diffusion model, the evolution of the concentration profiles in the growth direction is calculated in order to understand the energy shift of the optical phonons and the intensity decay of the folded acoustic phonons. The analysis of the latter provides values of the interdiffusion coefficient D^*. The strong dependence of the tracer-diffusion constants on the Si concentration causes different intermixing behavior of the Si and Ge layers, which results in a dependence of the interdiffusion coefficient on the degree of homogenization. A variation of D^* with the average Si content and the superlattice period is obtained and is compared to the standard interdiffusion analysis.

I. INTRODUCTION

Si/Ge superlattices (SL's) are currently of considerable interest due to their optical and electronic properties, especially the idea of creating semiconductors with a quasidirect energy gap.[1–4] The structural stability at high-temperature treatment is crucial for the integration of these structures into silicon technology. Furthermore, short-period SL's offer a possibility to study diffusion processes on a scale of the period length. Interdiffusion coefficients, which are, in the case of the Si/Ge system, of both technological and scientific interest, can be obtained by analyzing the evolution of the composition profile in the growth direction. Using x-ray diffraction, this has been applied to crystalline[5,6] and amorphous metals,[7] Si/SiGe and Si/Ge SL's,[8,9] and turned out to be several orders of magnitude more sensitive compared to conventional diffusion measurements, such as sputtering, Rutherford backscattering, and secondary-ion mass spectroscopy.[7] Diffusion lengths as low as 1 Å are observable. Hence considerably lower temperature regions can be examined. An alternative technique is Raman spectroscopy. We used this method to investigate Si/Ge SL's, considering the intensity decay of the folded first-order longitudinal acoustic (LA_1) phonon. Raman spectroscopy is a versatile, nondestructive, and sensitive technique for characterizing SL's. It provides detailed information on strain, layer thickness, and interface roughness.[10] The study of these quantities during thermal treatment leads to a more complete understanding of the intermixing process compared to x-ray-diffraction analysis on its own. An advantage is also the sensitivity of Raman scattering even for very thin SL's with total thicknesses below 300 Å.

The paper is organized in the following way. We first describe the samples and the experimental setup. In Sec. III the general features of SL Raman spectra are assembled. A simple atomistic diffusion model is then presented in Sec. IV, which serves to discuss the evolution of the optical modes in Sec. V. In Sec. VI we derive interdiffusion coefficients from the decay of the LA_1 mode and discuss their dependence on the sample parameters by comparison to interdiffusion theory. Finally strain effects are considered, followed by a summary of the results.

TABLE I. Structural data of the observed $(Si)_m/(Ge)_n$ superlattices. d_{Si} and d_{Ge} are the nominal layer thicknesses in units of monolayers.

Substrate (buffer)	d_{Si} (ML)	d_{Ge} (ML)	d_{tot} (Å)	Strain (%) Si	Strain (%) Ge
(100) Ge	3	9	300	4.2	0
(100) Ge	3	9	2000	3.7	−0.5
(100) Si (90-Å Ge)	12	12	670	2.1	−2.1
(100) Si (90-Å Ge)	8	8	670	2.1	−2.1
(100) Si (Ge +3/3 SL)	6	6	500	1.7	−2.5
(100) Si (90-Å Ge)	5	5	2300	2.1	−2.1
(100) Si (90-Å Ge)	3	3	1150	2.1	−2.1
(100) Si (130-Å Ge)	7	3	1400	1.4	−2.8

II. EXPERIMENT

The samples were grown by low-temperature molecular-beam epitaxy (MBE) on a Ge(100) substrate or a Si(100) substrate with periodicities of 6 to 24 monolayers (ML). Except for the $(Si)_3/(Ge)_9$ SL, all samples consisted of a strain-symmetrizing Ge buffer layer followed by the SL, thus avoiding the thickness limitation for pseudomorphic growth.[3] The sample parameters are listed in Table I. For details of the growth and characterization, see Refs. 11 and 12.

All Raman spectra were measured in a 100-(011/011)-$\bar{1}$00 backscattering geometry at room temperature using the 476.5- or 514.5-nm lines of an Ar^+ laser and a conventional Raman setup with a triple grating spectrometer equipped with a photodiode multichannel detector. The spectral resolution is about 6 cm^{-1}. For comparing intensities of different phonon modes, a careful adjustment of the polarization is essential, since they obey different Raman selection rules.[13] Only longitudinal modes are observed.

The samples were heated by irradiation in a quartz tube furnace under vacuum conditions. Heating and coiling times were negligible compared to annealing periods. The temperature was measured by a NiCr/Ni thermocouple located in the Si sample holder block.

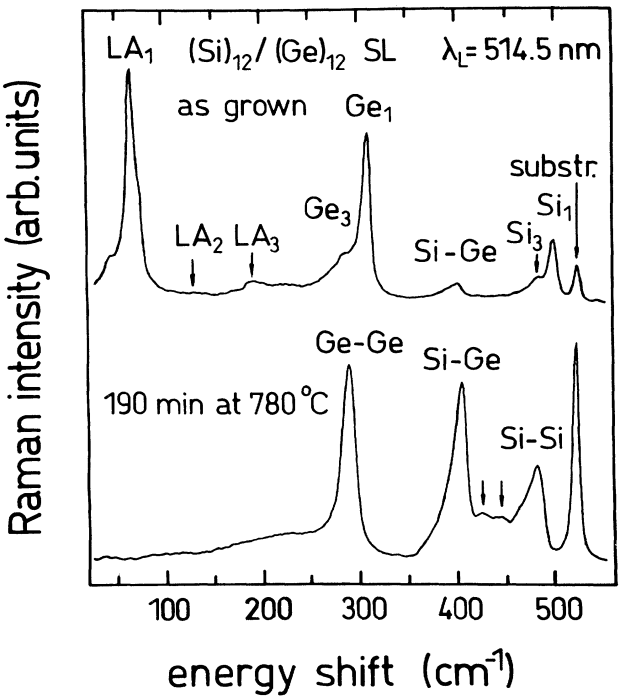

FIG. 1. Raman spectra of a $(Si)_{12}/(Ge)_{12}$ superlattice recorded with the 514.5-nm Ar line at 300 K from the as-grown sample and after 190 min of annealing at 780 °C (alloylike). Si_n,Ge_n denotes the confined optical modes, LA_n the folded acoustic modes.

III. RAMAN SCATTERING IN SUPERLATTICES

A typical Raman spectrum of a $(Si)_{12}/(Ge)_{12}$ SL is shown in Fig. 1. In the optical-phonon region, various peaks appear around 300 and 500 cm^{-1} originating from the Ge and Si layers, respectively. The splitting is due to phonon confinement effects, since the missing overlap of the corresponding Si and Ge optical-phonon dispersion curves does not allow the propagation of optical phonons in the adjacent layers. The mode energies can be explained by a simple "standing-wave" model.[14] Additionally the phonon positions are affected by the built-in strain.[10] The mode at 400 cm^{-1} is attributed to a Si-Ge alloylike vibration mainly attributable to the interface roughness of about 2 ML,[3] the intensity being, to first order, approximately proportional to the relative number of Si—Ge bonds.[15] At 520 cm^{-1}, a Si bulk phonon originating from the substrate appears due to the small SL thickness of 670 Å. In the acoustic region the artificial SL periodicity yields, via Brillouin-zone folding, as series of approximately equidistant phonon peaks, which are indicated by the arrows in Fig. 1.[16] Their intensities are expected to be proportional to the square of the corresponding Fourier components of the composition profile.[17] Here, for example, the second-order folded acoustic phonon, LA_2, is very weak, as expected for equal Si and Ge layer thicknesses for which the even Fourier components disappear.

The lower spectrum was recorded after annealing the sample for 190 min at 780 °C. The changes are drastic, demonstrating the sensitivity of the phonon spectra to intermixing. The disappearance of the folded LA phonons indicates the complete alloying of the sample. A typical three-mode behavior with phonons originating from local Si-Si, Ge-Ge, and Si-Ge vibrations, respectively, is observed.[15] The small peaks observed between the Si-Si and Si-Ge modes are also attributed to other typical alloy modes.[18] There is excellent agreement between the spectra of the thermally homogenized SL's and Raman measurements of corresponding liquid-phase-epitaxy (LPE)-grown alloys.[18] We therefore conclude that sufficient thermal treatment of Si/Ge SL's yields the corresponding alloys.

The transition between the two extreme cases of sharp interfaces and complete intermixing is shown in detail for a $(Si)_8/(Ge)_8$ SL in Fig. 2. The first spectrum originates from the as-grown sample. Starting with an annealing step of 25 min at 657 °C, the overall annealing time was doubled between each Raman measurement, while the temperature was kept constant throughout. The last spectrum was recorded after a final 190-min 780 °C treatment. The mode intensities were normalized to the Ge phonon, because the Raman resonance profile of this SL mode is rather similar to the LA_1 and Si-Ge mode. This is due to the less-pronounced confinement of the Ge mode compared to the Si mode.[19] As the acoustic modes propagate throughout the whole SL and the optical modes are more or less confined to the individual layers or to the interface region, they are likely to have different resonance behavior. In addition, the electron-phonon coupling for acoustic and optical modes can be very

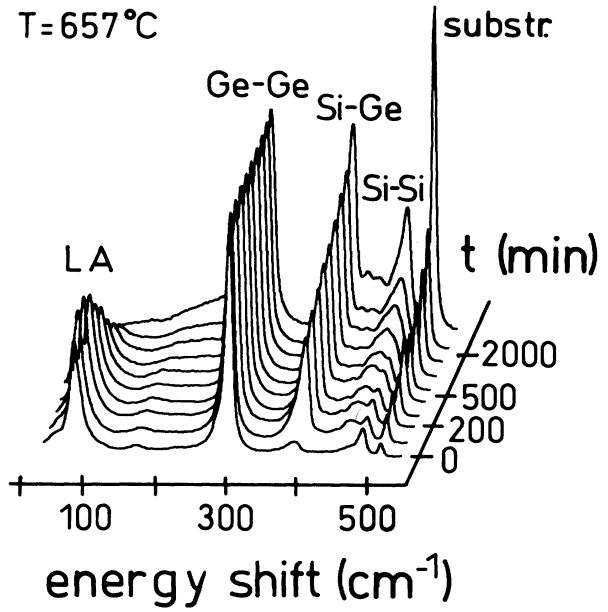

FIG. 2. Series of Raman spectra of a $(Si)_8/(Ge)_8$ SL, recorded at 514.5 nm. Starting with a 25-min anneal, the annealing time was subsequently doubled between each spectrum.

different, which also affects the resonance behavior. Therefore the Raman intensities of the different modes may change, as long as the intermixing process alters the band structure. All samples were measured at two different laser lines in order to control these resonance effects. For example, out of resonance we expect from theory a monotonic intensity decay of the LA_1 phonon due to its correlation with the composition profile. However, for the laser wavelength of 514.5 nm, the mode initially increases in intensity. We believe this is due to the described resonance effect, since it depends on the excitation wavelength. We found that for the LA_1 mode primarily the early stages of mixing are affected, while in the case of the Si-Ge mode no such effect was observed. The acoustic phonons are discussed in detail in Sec. VI.

A characteristic feature is the pronounced rise of the Si-Ge mode caused by an increase of the number of Si—Ge bonds due to interface smearing. In fact, the Si-Ge phonon turned out to be the most sensitive probe of intermixing, as can be seen after the first heat treatment step of the $(Si)_8/(Ge)_8$ SL where the Si-Ge mode drastically increases in intensity although the rest of the spectrum remains nearly unchanged. Due to this sensitivity and to the absence of resonance effects, the relative Si-Ge mode intensity is a sensitive measure of the degree of intermixing. In a study of the initial stage of intermixing, a 10% intensity rise for this sample was already observed after only a 40-min annealing step at 450 °C. The other samples showed an initial increase for temperatures of 540–630 °C. We found that the relative sensitivity to thermal treatment during the initial stage of diffusion is correlated to the fraction of interfacial atoms within the SL, i.e., high-quality samples are more sensitive. A detailed discussion of this effect is to be published elsewhere.[20]

We observe an increase in intensity of the Si bulk phonon during annealing. This is due to the lower absorption of the alloy compared to the corresponding SL. At the low-energy side of the Si phonon, an additional mode appears during annealing, which was first reported by Brugger *et al.*[10] In Fig. 3 the shift of the peak positions of the optical modes is plotted versus the intensity ratio of the Si-Ge mode to the Ge mode, which corresponds to the stage of homogenization. The left-hand side corresponds to the as-grown sample and the right-hand side to the completely alloyed one. We see that the original Si mode remains almost constant, while the additional one starts at a considerably lower energy and then shifts up. In contrast, the energy of the Si-Ge mode lowers finally after a pronounced initial rise. The Ge mode shows no splitting and the energy decreases monotonically.

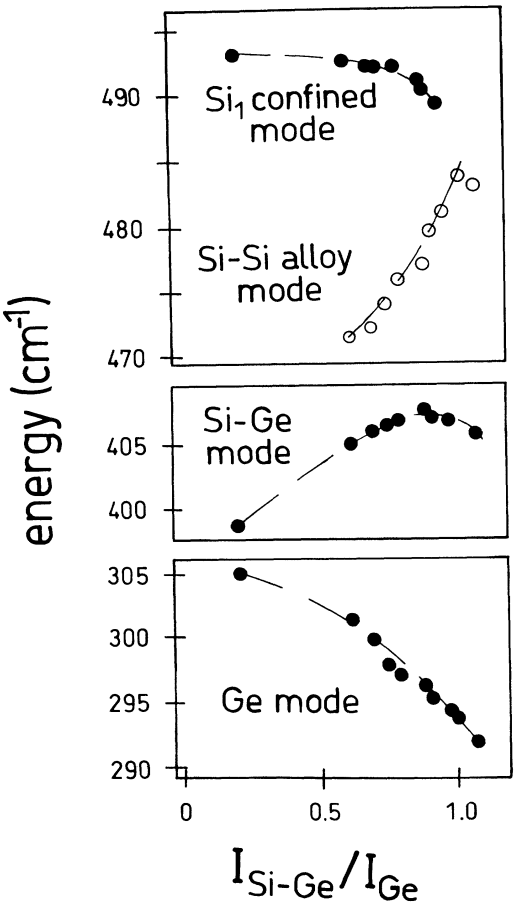

FIG. 3. Energy shift of the optical-phonon modes of a $(Si)_8/(Ge)_8$ SL at various stages of intermixing. The points furthest to the left correspond to the as-grown sample and the points furthest to the right correspond to the completely alloyed sample. This convention is also used in subsequent similar figures.

IV. INTERDIFFUSION MODEL

In order to understand the changes of the phonon spectrum, we use a simple microscopic interdiffusion model that provides the evolution of the composition profile in the growth direction. It is assumed that every atom in the diamond lattice can exchange its site statistically with one of its four nearest neighbors according to a given "hopping" probability. First the agreement of this assumption with the macroscopic linear interdiffusion theory[5] was tested. Analyzing the composition profiles by fast Fourier transformation (FFT), we obtain the predicted exponential decay of the square of the first Fourier component versus time. Also the expected square dependence of the decay rate on the SL period is reproduced correctly. Furthermore, we found that the correlation between the decay rate and the hopping probability was linear. This means that the latter corresponds to a macroscopic interdiffusion coefficient. In order to represent the features of the Si/Ge system correctly in the following calculations, the hopping rate was given a suitable value dependent on the average Si content of the (100) monolayer in which the atom is located. Thus we take into account the fact that the tracer-diffusion constants of both Si and Ge atoms in SiGe alloys decrease by about six orders of magnitude as the composition is altered from pure Ge to pure Si.[21] For a given composition, the tracer diffusivities of Si and Ge atoms are equal within one order of magnitude,[22] and so the hopping rate was chosen identical for both.

Figure 4 shows the evolution of a composition profile of a $(Si)_8/(Ge)_8$ SL with an initial interface roughness of 2 ML, resulting in a rather homogeneous intermixing of the Ge layers, whereas the core of the Si layers and the sharpness of the interfaces are preserved for a long time. So the Si layers can be treated as pure but narrowing slabs, while the Ge layers can be treated as an alloy with increasing Si content.

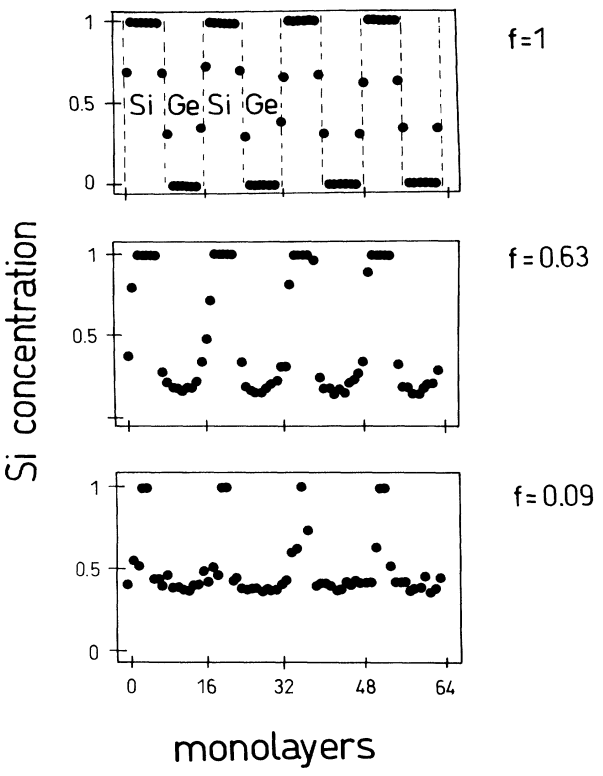

FIG. 4. Calculated concentration profiles of a $(Si)_8/(Ge)_8$ SL based on an initial state with slightly smeared interfaces. f gives the first Fourier component of the profile describing the progress of intermixing.

V. SHIFT OF THE OPTICAL MODES

From Fig. 4 it can be seen that the high-energy Si mode originates from the pure Si cores while the other peak originates from the Si—Si bonds of the Si-enriched Ge layers.[10] Optical-phonon energies of partially homogenized SL's are explained by the following model. Each (100) bilayer makes an alloylike contribution to each optical mode with an energy that depends on the average Si content of the bilayer, weighted by the corresponding fraction of Si—Si, Si—Ge, and Ge—Ge bonds between the constituent monolayers of the bilayer, respectively. The dependence of the optical-phonon energies on the Si fraction in unstrained SiGe alloys can be taken from Refs. 15 and 18. The value of the lattice parameter is constant throughout the whole SL and is not changed by intermixing, whereas in the case of an unstrained alloy the intrinsic lattice constant varies with composition. Therefore we have to take this into account by correcting the data for the energy shift induced by the different strain. The strain shift taken from Refs. 14 and 23 yields the result shown in Fig. 5, where we plot the relative composition-dependent energy shift of the optical alloy modes versus Si content, assuming a fixed composition-independent lattice constant. The absolute energy scale is given by the choice of the latter, in our case the lattice constant of the SL. The model is only valid for advanced stages of intermixing when the confinement effect caused by the individual layer thickness becomes negligible. We can now explain the upward shift of the alloylike Si-Si mode in the course of intermixing by the change in energy of the corresponding alloy mode with increasing Si content. The other mode remains almost constant as it originates from the stable Si core slabs. Its slight downshift is probably due to the layer narrowing, which lowers the energy of the confined modes.

The evolution of the Ge mode, on the other hand, is quite different (Fig. 3). The energy decreases linearly and no splitting is observed. This is due to the rather homogeneous Si enrichment of the Ge layers, whose increasing Si content shifts the mode position downwards. The other samples show a similar behavior.

The shift of the Si-Ge mode of various samples is plot-

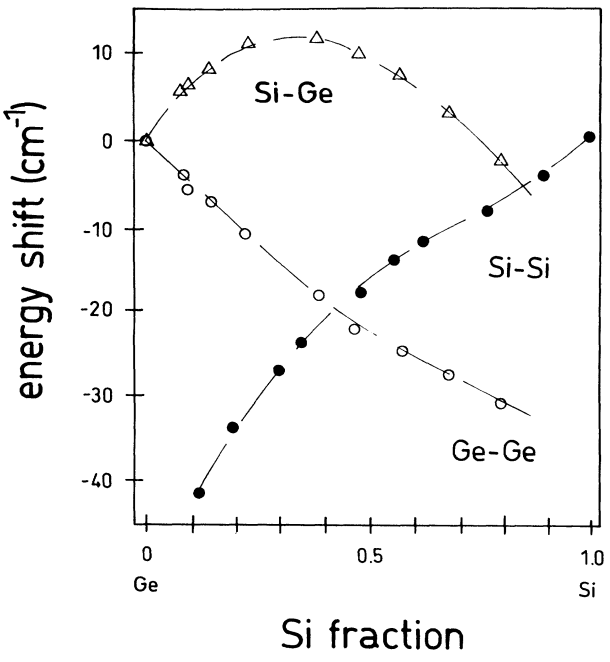

FIG. 5. Composition-dependent energy shift of the optical alloy modes calculated from Ref. 15 assuming a composition-independent lattice constant. The absolute energy values are given by the choice of the latter.

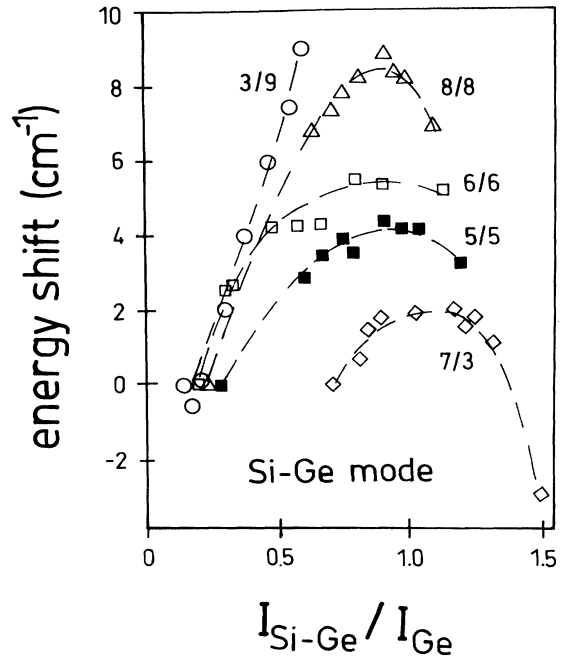

FIG. 6. Energy shift of the Si-Ge mode of various SL's vs the degree of intermixing.

ted in Fig. 6. Initially we see an upward shift in energy, which in the case of the Si-rich SL's reaches a maximum, followed by a decrease with further intermixing. The $(Si)_7/(Ge)_3$ SL shows the largest final downshift. In partially mixed SL's, two regions contribute to the SiGe mode: the interface area and the Si-enriched Ge layers. The energy of the first contribution cannot be described in the simple model if the concentration profile is as sharp as in the case of the studied samples. However, we can assume that the energy depends only on the lattice constant and not on the Si/Ge ratio, if the interface quality is comparable for all samples.[23] From Fig. 5, the alloylike contribution can be estimated in the same way as was performed for the Si and Ge mode previously. Although we are not able to describe the initial Si-Ge mode energy, we can understand the behavior beyond the stage of mixing where the contribution of the Ge layers begins to dominate. Due to the increasing Si content in the Ge layers the mode energy shifts approximately along the parabola until the overall average Si content of the SL is reached. Hence in the case of the $(Si)_3/(Ge)_9$ SL the shift is monotonic due to the average Si fraction of only 25%, which precludes the energy maximum being reached. On the other hand, in the more Si-rich SL's the maximum is reached and the mode energy finally shifts downwards. The effect is more pronounced for the $(Si)_7/(Ge)_3$ SL due to the higher Si content. These results support the assumption that the main contribution to the Si-Ge mode in advanced stages of homogenization originates from the Si-enriched Ge layers. In summary, we have seen that the optical modes behave like local probes, since they are originating from different regions of the SL, providing detailed information on the development of the composition profile.

VI. ACOUSTIC MODES

A confirmation for the calculated development of the profile is given by the evolution of the intensity ratio between the LA_2 and LA_1 modes versus annealing time in Fig. 7, where a pronounced rise is seen. We note that the initial existence of a LA_2 mode for the SL's with equal Si and Ge layer thicknesses might be due to a slightly asymmetric composition profile caused by different growth conditions on Si and Ge surfaces. Assuming a proportionality of the folded acoustic-phonon intensities to the square of the corresponding Fourier components, we can understand the observed rise by Fourier analysis of the profiles. This shows an initial increase of the second Fourier component compared to the first one due to the asymmetric evolution of the profile. Numerical solutions of the nonlinear diffusion equation show similar results.[24]

We observed no energy shift of the LA_1 mode due to the fact that the SL periodicity is not affected by intermixing. However, the LA_1 mode intensity is of special interest, because an analytical correlation between the first Fourier component A and the bulk interdiffusion coefficient D_∞ can be derived:[25]

$$\frac{\partial}{\partial t}\ln\left[\frac{A^2(t)}{A^2(0)}\right]=-2k^2D_\infty\left[1+\frac{2\kappa k^2}{f_0''}\right]=-2k^2D^*\ , \tag{1}$$

where κ is the gradient energy coefficient f_0'' is the second derivative of the Helmholtz free energy with respect to the composition x, $k=2\pi/d$, where d is the SL period, and D^* is the period-length-dependent interdiffusion coefficient. From theory an exponential decay of $A(t)$ is expected if D_∞ is composition independent. The gradient energy term is additional to the standard diffusion analysis, and is important for large concentration gradients, i.e., when the composition varies on an atomic scale, and is due to a finite energy of mixing. Neglecting the gradient energy we see an inverse square dependence of the decay rate on the SL period. It has been shown that[26]

$$D_\infty=[xD_{\mathrm{Ge}}+(1-x)D_{\mathrm{Si}}]F\ ;\quad F=x(1-x)f_0''/Nk_BT\ , \tag{2}$$

where $D_{\mathrm{Ge}}, D_{\mathrm{Si}}$ are the tracer diffusivities of Si and Ge atoms in an alloy with a Si fraction x, N is the atomic density, k_B is the Boltzmann constant, and T is the absolute temperature. The formula means that the interdiffusion constant is a weighted average of the tracer values, multiplied by a factor depending on thermodynamic parameters of the system. The main contribution to F provides the energy of mixing, as seen later.

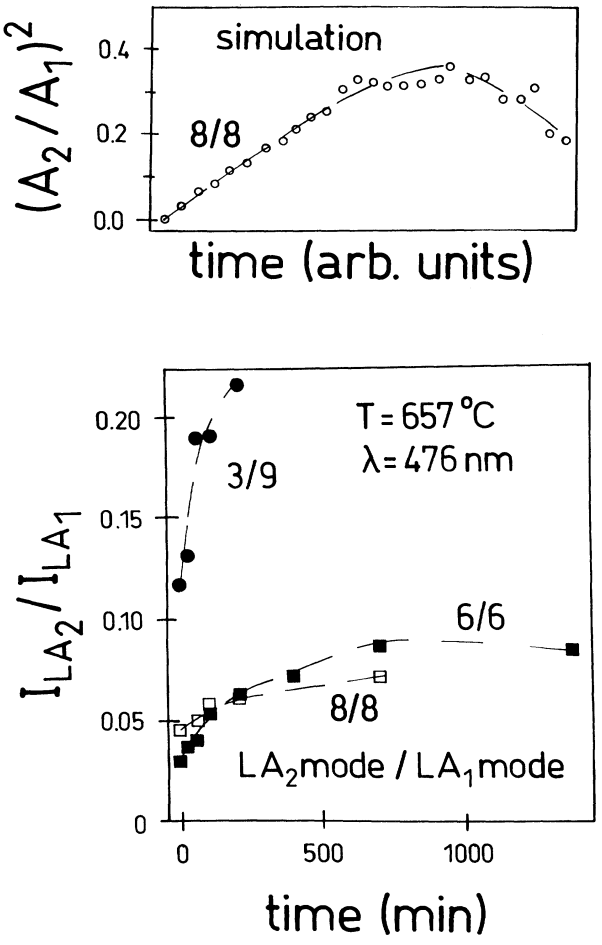

FIG. 7. Intensity ratio between the second- and first-order folded acoustic phonons vs annealing time for various samples. n/m denotes the number of Si and Ge monolayers, respectively. The upper part shows the ratio of the square of the second and first Fourier components vs time calculated with the model described in the text.

In Fig. 8 the decay of the logarithm of the LA_1 mode intensity versus annealing time is shown. The intensities were normalized to the intensity of the Ge phonon as discussed above. We observe a near-linear decay for the $(Si)_3/(Ge)_9$ SL's, whereas the curves of the others show a bending. According to (1) the slope of the decay should be proportional to D^*. We believe that the deviation from the theoretically predicted linear behavior is caused by the above-mentioned strong composition dependence of the tracer diffusivities. As shown in Fig. 4, initially diffusion mainly occurs in the Ge layers where the diffusivity is much higher, while in subsequent stages the rising Si content slows down the diffusion process there, resulting in a smaller decay rate of the LA_1 phonon. The slowing down is more pronounced with increasing overall Si fraction of the SL. As a consequence, we expect the initial slope to be similar for samples of comparable quality but the final slope to be flatter for more Si-rich SL's. Indeed we observe a more or less linear decay of the Ge-rich $(Si)_3/(Ge)_9$ SL. Our explanation is also supported by the simulation calculation shown in Fig. 8, where a more pronounced slowing down of a $(Si)_7/(Ge)_3$ SL compared to a $(Si)_3/(Ge)_7$ SL is seen. Numerical solutions of the nonlinear diffusion equation with a composition-dependent D_∞ qualitatively produce the same bending of the curves.[24] Another consequence is that the initial decay rate should depend on the sample quality. We expect the initial slope to be flatter for SL with smeared interfaces. Calculations comparing a SL with an ideal square-wave profile to one with a sinusoidal profile support this consideration. We note that the attribution of the nonlinearity to strain relaxation effects, as discussed for x-ray interdiffusion measurements in Refs. 8 and 27, is not valid for our samples, because they are strain symmetrized, which excludes relaxation during annealing [except for the $(Si)_3/(Ge)_9$ SL's, as will be discussed later].

These results lead to the conclusion that reasonable interdiffusion coefficients can only be evaluated from the final slopes. A similar annealing experiment at 725 °C was performed after preannealing the samples until the LA_1 intensity was reduced to one-quarter of its original value, in order to ensure that we started our analysis in the region of linearity that corresponds to the last two or three points in Fig. 8. The decay rates thus obtained were much more closely linear than before. From this

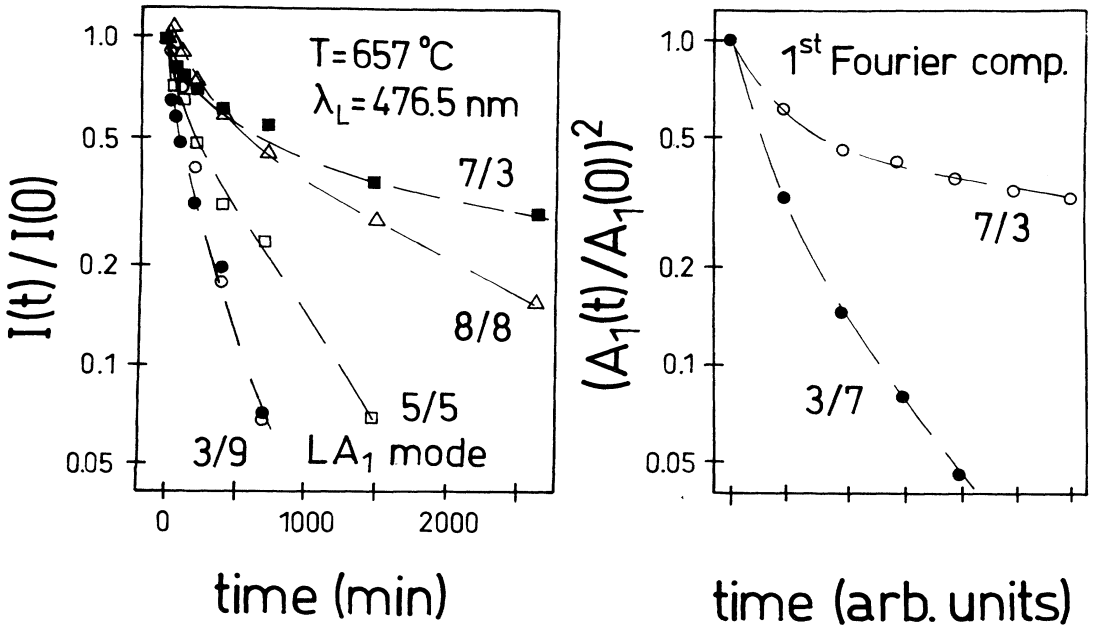

FIG. 8. The left-hand side shows the intensity of the LA_1 mode normalized to the Ge mode vs annealing time for different SL's. The vertical axis is scaled logarithmically. The right-hand side shows the simulated decay of the square of the first Fourier component of a $(Si)_3/(Ge)_7$ and a $(Si)_7/(Ge)_3$ SL.

data, interdiffusion coefficients D^* are obtained according to (1). Measurements at different temperatures allowed a rough estimation of the activation energies, which were found to be somewhere between 3 and 4 eV. This is in agreement with the x-ray interdiffusion measurements on Si/Ge SL's by Chang *et al.*[8] but differs from a similar analysis by Baribeau, Pascual, and Saimoto,[27] where values between 0.5 and 2 eV are reported. The tracer activation energies in Si-Ge alloys increase monotonically from 3 eV in pure Ge to 5 eV in pure Si.[21] The activation energy of the interdiffusion coefficient D^* can also be derived form this data by[28]

$$E_a^* = xE_a^{\mathrm{Si}} + (1-x)E_a^{\mathrm{Ge}} - k_B T(F-1)/F \ , \qquad (3)$$

where $E_a^{\mathrm{Si}}, E_a^{\mathrm{Ge}}$ are the activation energies of Si and Ge tracer atoms in an alloy with Si content x. In the regular solution model f_0'' can be approximated by $f_0'' = RT/(1-x)x - 2L_A zV$, where R is the universal gas constant, L_A is Avogadro's number, and z is the coordination number.[7] V is the energy of mixing, which was measured to be $+10$ meV.[29] Thus the Si/Ge system is phase separating. The small but positive value of V should cause a miscibility gap below 200 K (Ref. 30), which cannot be observed due to the negligible atomic mobility at this temperature. For $x = 0.5$ and $T = 690$ °C, we obtain $f_0'' = 1.8 \times 10^9$ J/m^3. The temperature-dependent term in (3) is then -26 meV. We see that the activation energy for a phase-separating system increases, but the amount is negligible for Si/Ge. Therefore we expect deviations from alloy tracer activation energies to be mainly due to strain effects.

In Fig. 9, interdiffusion coefficients of various samples

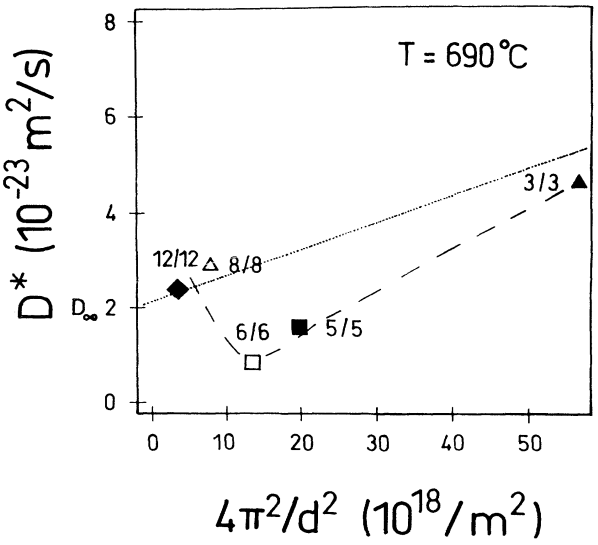

FIG. 9. Interdiffusion coefficient vs inverse square of the SL periodicity d. The dashed line is a guide to the eye for experimental points, while the dotted line gives the theoretical first-order approximation.

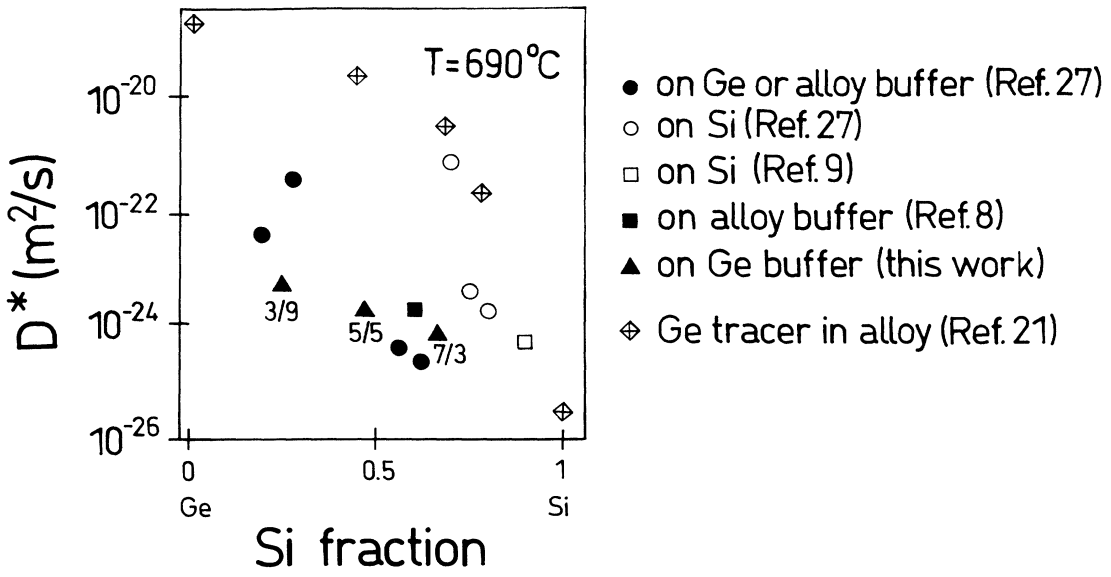

FIG. 10. Interdiffusion coefficient D^* at 690 °C vs Si content. For comparison the results obtained by other groups are also given. Open symbols denote growth on Si; solid symbols denote growth on Ge or Si-Ge alloy buffers.

with equal Si/Ge ratio but different period lengths, d, are plotted versus $1/d^2$. The values were interpolated to 690 °C. We see an enhancement of D^* for short periods, whereas a minimum is observed at $d=12$ ML. In a first-order approximation from theory a linear dependence of D^* on $1/d^2$ as given in (1) is expected. Considering only next-neighbor interactions we obtain[8] $\kappa=Na^2V/8$ for a diamond lattice in a (100) direction, where N is the atomic density and a is the lattice constant. This yields $\kappa=2.2\times10^{-11}$ J/m. Assuming a bulk value $D_\infty=2.0\times10^{-24}$ m²/s (which is D^* for $d\rightarrow\infty$) we obtain a dependence as indicated by the dotted line drawn in Fig. 9. The obvious deviation from linearity might be caused by the fact that in (1) only the dependence of the Helmholtz free energy on the second derivative of ∂x with respect to ∂z is considered (x, Si fraction; z, axis in growth direction). Taking into account additional higher-order terms yields a nonlinear dependence of D^* on $1/d^2$.[31] A period-length dependence of D^* similar to that shown here is reported for crystalline Cu/Ni systems.[31] As a result we find that the period-length dependence of D^* is important for SL's with $d<20$ ML.

In Fig. 10 we plot the values of D^* at 690 °C for three SL's with similar period but different Si/Ge ratio, versus Si content. For comparison data interpolated from Refs. 8 and 27 are also shown. We observe a decrease of D^* with increasing Si fraction. The pronounced fluctuation of the data is probably caused by the fact that samples are grown on different substrates and hence may have significantly different strain distributions and dislocation densities. These parameters influence diffusion, as discussed later. Additionally, the Ge tracer-diffusion coefficients from Ref. 27 measured in Si-Ge alloys above 1000 °C are also shown. These have been extrapolated down to 690 °C. The trend is similar, whereas the deviation between the absolute values is considerable. The correlation between interdiffusion coefficient and tracer-diffusion coefficients is given by (2). For $x=0.5$ and $T=690$ °C, we obtain $F=0.75$. This means that $F\approx1$ and hence the interdiffusion coefficient of a Si/Ge system is simply given by a weighted average of the Si and Ge tracer diffusivities, which are almost equal. We believe that the large discrepancy between the bulk and interdiffusion measurements is due to the uncertainty of the tracer measurements (one order of magnitude) and especially to the extrapolation over a temperature range as wide as 400 °C. In this case, smaller activation energies of the SL interdiffusion would explain the deviation.

VII. STRAIN EFFECTS

Two $(Si)_3/(Ge)_9$ SL's with identical composition but different thicknesses of 300 and 2000 Å, respectively, were examined. Both samples were grown on a Ge substrate. Low-energy electron-diffraction (LEED) measurements showed that the latter had already partially relaxed during growth so that the strain of the Si layers was reduced to $\approx3.7\%$, whereas the first one is pseudomorphic to the Ge substrate. Raman spectroscopy is also sensitive to strain relaxation. In Fig. 11 we consider the energy shift of the optical modes of the $(Si)_3/(Ge)_9$ SL's during the thermal treatment at 657 °C. The initial

upward shift of the energy of all modes in the case of the thick SL is due to a further strain relaxation. Using the strain dependence of SL phonons,[14,23] we derive a nearly complete strain relaxation after the first 25-min annealing step, while the thin SL shows no signs of strain relaxation. This is due to the fact that the latter is thermodynamically stable, whereas the other sample exceeds the critical thickness.[3] First hints on a relaxation of the thick sample were obtained after a 40-min anneal at 450 °C. In addition to the energy shift, a change in the relative optical-phonon intensities was observed. This effect is not caused by diffusion, as a subsequent treatment at 500 °C left the spectrum unchanged. We attribute it to a relaxation process, since the Raman resonance profiles of these $(Si)_3/(Ge)_9$ SL's show a pronounced dependence on strain.[32] The other SL's are stable due to the strain-symmetrizing buffer layer.

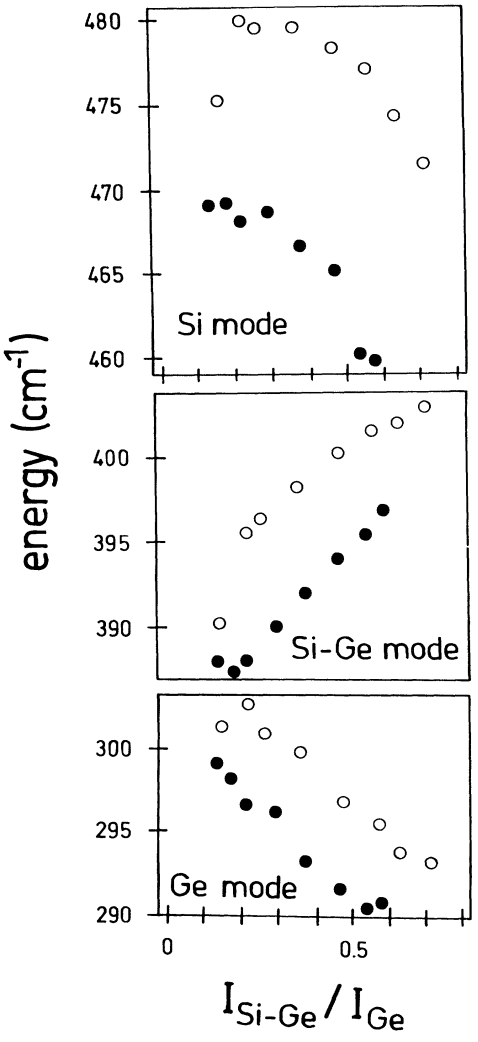

FIG. 11. Energy shift of the optical phonons of a fully strained (solid circles) and a partially relaxed (open circles) $(Si)_3/(Ge)_9$ SL during intermixing.

Despite the different strain distribution, no significant differences in the LA_1 mode decay of the $(Si)_3/(Ge)_9$ SL's were observed, as is evident from Fig. 8. Therefore, for Ge-rich SL's with lattice constants close to Ge, strain effects on D^* seem to be negligible. In this context an analysis formulated by Cahn[33] is often used to treat strain effects on diffusion. An expression $+(2\eta^2/f_0'')Y$ as well as the gradient energy term in (1) is included, where η is the relative mismatch of the lattice constants (Si/Ge system: 0.04) and Y is a generalized elastic modulus. This would indicate that a lattice mismatch between the components enhances diffusion compared to the bulk tracer diffusivities. However, this analysis has to be handled with care, because the elastic energy contribution to the bulk free energy f_0 is not included. Work by Cook and DeFontain,[34] which includes this term, showed that, in contrast, phase separation is usually favored by elastic energy contributions. It should be pointed out that these considerations only reflect the thermodynamic point of view, while the influence of strain on D_{Si} and D_{Ge}, for example on the activation energy, is not treated at all. The enhanced interdiffusion for Si-rich pseudomorphic SL's on the Si-substrate compared to the alloy-buffer-grown samples seen in Fig. 10 could be due to this. Also this analysis does not tell us anything about the influence of the strain distribution on D^*, which one would need to know, for instance, in order to compare our two $(Si_3)/(Ge_9)$ SL's. Therefore, the effects of strain on the interdiffusion processes still remain unclear both from the theoretical and the experimental point of view and so further studies are necessary.

VIII. SUMMARY

In summary, we have demonstrated that Raman spectroscopy is a versatile and sensitive technique for characterizing annealing effects on Si/Ge SL's. The energy shift of the optical-phonon modes was explained by considering the concentration profiles calculated on the basis of a simple microscopic diffusion model. The main feature of the intermixing process is the relative stability of the Si layers, whereas the Ge layers enrich homogeneously with Si. This effect causes a dependence of the interdiffusion on the degree of homogenization. Consequently, interdiffusion coefficients were derived from the final slopes of the LA_1 mode decay. We also showed that the period length dependence due to the gradient energy has to be considered when $d < 20$ ML. Finally, as expected from the tracer diffusivities, a rising Si content results in lower interdiffusion.

ACKNOWLEDGMENTS

We would like to thank U. Menczigar for fruitful discussions on resonant Raman scattering.

[1]K. Eberl, W. Wegscheider, E. Friess, and G. Abstreiter, in *Heterostructures on Silicon: One Step Further with Silicon,* edited by Y. I. Nissim and E. Rosencher (Kluwer Academic, Boston, 1989), p. 153.
[2]G. Abstreiter, K. Eberl, E. Friess, W. Wegscheider, and R. Zachai, J. Cryst. Growth **95**, 431 (1989).
[3]E. Kasper, H. Kibbel, H. Jorke, H. Brugger, E. Friess, and G. Abstreiter, Phys. Rev. B **38**, 3599 (1988).
[4]T. P. Pearsall, Crit. Rev. Solid State Mater. Sci. **15**, 551 (1989).
[5]J. DuMond and J. P. Youtz, J. Appl. Phys. **11**, 357 (1940).
[6]H. E. Cook and J. E. Hilliard, J. Appl. Phys. **40**, 2191 (1969).
[7]A. L. Greer and F. Spaepen, in *Synthetic Modulated Structures,* edited by L. L. Chang and B. C. Giessen (Academic, Orlando, 1985), p. 419
[8]S. J. Chang, K. L. Wang, R. C. Bowman, and P. M. Adams, Appl. Phys. Lett. **54**, 1253 (1989).
[9]S. M. Prokes and K. L. Wang, Appl. Phys. Lett. **56**, 2628 (1990).
[10]H. Brugger, E. Friess, G. Abstreiter, E. Kasper, and H. Kibbel, Semicond. Sci. Technol. **3**, 1166 (1988).
[11]K. Eberl, E. Friess, W. Wegscheider, U. Menczigar, and G. Abstreiter, Thin Solid Films **183**, 95 (1989).
[12]K. Eberl, W. Wegscheider, and G. Abstreiter, J. Cryst. Growth (to be published).
[13]R. Loudon, Adv. Phys. **13**, 423 (1964).
[14]E. Friess, K. Eberl, U. Menczigar, and G. Abstreiter, Solid State Commun. **73**, 203 (1990).
[15]M. A. Renucci, J. B. Renucci, and M. Cardona, in *Proceedings of the 2nd International Conference on Light Scattering in Solids,* edited by M. Balkanski (Flammarion, Paris, 1971), p. 326.
[16]H. Brugger, G. Abstreiter, H. Jorke, H. J. Herzog, and E. Kasper, Phys. Rev. B **33**, 5928 (1986).
[17]C. Colvard, T. A. Gant, M. V. Klein, R. Merlin, R. Fischer, H. Morkoc, and A. C. Gossard, Phys. Rev. B **31**, 2080 (1985).
[18]M. I. Alonso and K. Winer, Phys. Rev. B **39**, 10056 (1989).
[19]F. Cerdeira, M. I. Alonso, D. Niles, M. Garriga, M. Cardona, E. Kasper, and H. Kibbel, Phys. Rev. B **40**, 1361 (1989).
[20]E. Friess, R. Schorer, K. Eberl, and G. Abstreiter (unpublished).
[21]J. L. McVay and A. R. Ducharme, Phys. Rev. B **9**, 627 (1974).
[22]J. Räisänen, J. Hirvonen, and A. Anttila, Solid State Electron. **24**, 333 (1981).
[23]E. Friess, R. Schorer, K. Eberl, and G. Abstreiter (unpublished).
[24]T. Tsakalakos, Scr. Metall. **20**, 471 (1986).
[25]J. W. Cahn and J. E. Hilliard, J. Chem. Phys. **28**, 258 (1958).
[26]L. S. Darken, Trans. Am. Inst. Min. Metall. Pet. Eng. **175**, 184 (1948).
[27]J.-M. Baribeau, R. Pascual, and S. Saimoto, Appl. Phys. Lett. **57**, 1502 (1990).
[28]J. E. Reynolds, B. L. Averbach, and M. Cohen, Acta Metall. **5**, 29 (1957).
[29]V. T. Bubelik, S. S. Gorelik, A. A. Zaitsev, and A. Y. Polyakov, Phys. Status Solidi B **66**, 427 (1974).
[30]T. Soma, Phys. Status Solidi B **98**, 637 (1980).
[31]T. Tsakalakos, Thin Solid Films **86**, 79 (1981).
[32]G. Abstreiter, K. Eberl, E. Friess, U. Menczigar, W. Wegscheider, and R. Zachai, in *Spectroscopy of Semiconductor Microstructures,* Vol. 206 of *NATO Advanced Study Institute Series E: Applied Sciences,* edited by G. Fasol, A. Fasolino, and P. Lugli (Plenum, New York, 1989), p. 165.
[33]J. W. Cahn, Acta Metall. **9**, 795 (1961).
[34]H. E. Cook and D. DeFontain, Acta Metall. **19**, 607 (1971).